

# ANALYTICAL METHODS USED IN THE DESIGN OF THERMAL TOOLBOX ELEMENTS FOR EXTREME ENVIRONMENTS

David C. Bugby and Jose G. Rivera

Jet Propulsion Laboratory, California Institute of Technology

## ABSTRACT

This paper describes the analytical methods used in the design/development of new thermal toolbox elements for science payload operation/survival in extreme environments. These new thermal tools were developed as a result of five JPL projects (PALETTE, ARTEMIS, ROD-TSW, ES-ROD-TSW, and mini-ROD-TSW) and include thermally-switched enclosures (TSE), parabolic reflector radiators (PRR), spacerless multilayer insulation (SMLI), low conductance thermal isolators (LCTI), 3 types of reverse-operation DTE thermal switches (ROD-TSW), miniaturized loop heat pipes (mini-LHP), Vectran tension cables (VTC), and wire heat leak minimization (WHLM) techniques. The analytical methods are used to predict key performance parameters (KPPs) associated with each thermal tool. The KPPs include TSE lunar night heat loss flux ( $q_{\text{LOSS}}$ ), PRR lunar noon radiative sink temperature ( $T_s$ ), SMLI effective emissivity ( $\epsilon^*$ ), LCTI thermal conductance ( $G$ ), ROD-TSW/mini-LHP ON/OFF behavior, VTC structure stiffness and frequency ( $k$  and  $\nu$ ), and WHLM heat loss. The paper also describes thermal toolbox mission infusion status.

## NOMENCLATURE, ACRONYMS, ABBREVIATIONS\*

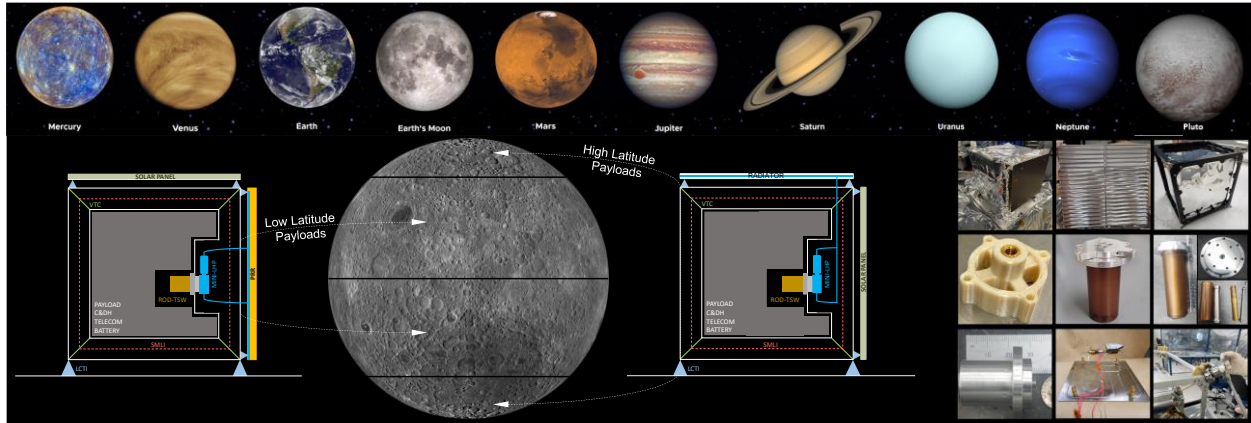
ARTEMIS	Architecture for Thermal Enclosures of Moon Instrument Suites
DTE	Differential Thermal Expansion
ES-ROD-TSW	Extended Stroke Reverse-Operation DTE Thermal Switch
mini-LHP	Miniaturized Loop Heat Pipe
mini-ROD-TSW	Miniaturized Reverse-Operation DTE Thermal Switch
PALETTE	Planetary and Lunar Environment Thermal Toolbox Elements
ROD-TSW	Reverse-Operation DTE Thermal Switch
VTC	Vectran Tension Cable
WHLM	Wire Heat Leak Minimization

\* *additional terms defined in the Appendix*

## INTRODUCTION

The desire for extended-duration robotic exploration in extreme environments like the Moon (without radioisotopes) has highlighted a need for improved thermal capabilities. The needs include better tools, advanced thermal architectures, and methods that enable tool scalability, extensibility, and planetary use. JPL has been working for the last 5 years in those areas (on the PALETTE<sup>1-3</sup>, ARTEMIS<sup>4</sup>, ROD-TSW<sup>5</sup>, ES-ROD-TSW<sup>6</sup>, and mini-ROD-TSW<sup>6</sup> projects) and this paper describes the thermal tools and their associated analytical methods. Remarkably, these new thermal tools are already being infused into missions such as the Farside Seismic Suite (FSS<sup>7</sup>), the Lunar Surface Electromagnetics Experiment at Night (LuSEE-Night<sup>8</sup>), and potentially many others.

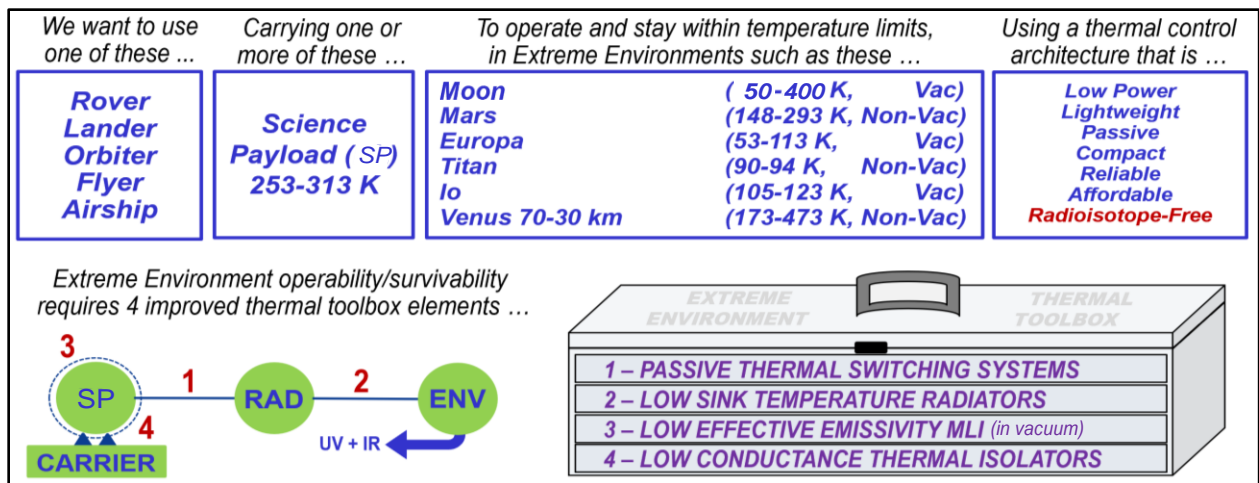
The extreme destinations in question are depicted graphically in Figure 1 along with lunar architectures at low/high latitudes and preview photos of nine of the ten thermal tools to be introduced later. The remainder of this paper is organized as follows. First, the **Problem** of science payload thermal control in extreme environments is presented along with the four basic thermal toolbox elements (passive thermal switches, low sink temperature radiators, radiative isolators, and conductive isolators). Next, the ten new additions to the thermal **Toolbox** are described. Following the toolbox section is a section describing the key analytical **Methods**. The final section of the paper provides details on thermal toolbox mission **Infusion**.



**Figure 1.** Extreme environment destinations, lunar architectures, and thermal tools.

**PROBLEM**

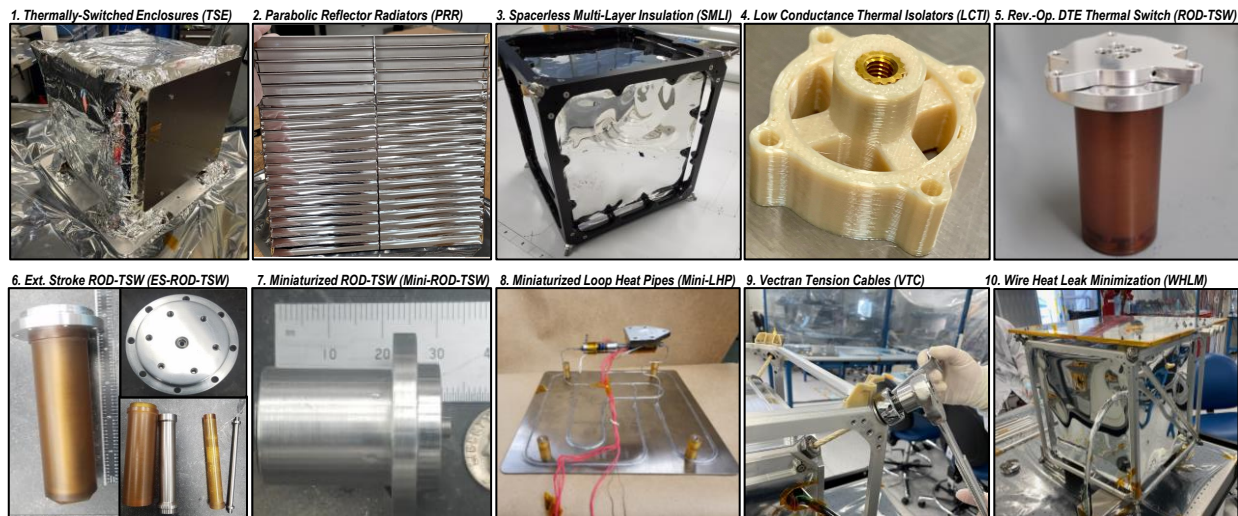
The overarching problem addressed in this paper, as depicted in Figure 2, is science payload (SP) thermal control in extreme environments. To maintain SPs within limits on different carriers at various extreme destinations, given typical constraints, requires a thermal architecture composed of a passive thermal switching system, a low sink temperature radiator, and high performance radiative/conductive isolation. While the architecture is not new, the thermal tools as well as the analytical methods to design and predict tool performance, are indeed new.



**Figure 2.** Problem of science payload control in extreme environments.

## TOOLBOX

The ten new additions to the thermal toolbox<sup>9-13</sup>, as illustrated in Figure 3, include the following: **(1) thermally-switched enclosures (TSE)**, which combine a passive thermal switching/transport system, a low sink temperature radiator, high performance radiative isolation, and high performance conductive isolation; **(2) parabolic reflector radiators (PRR)**, which are side-facing radiators on lunar surface SPs that reflect away lunar surface IR for a low sink temperature; **(3) spacerless multilayer insulation (SMLI)**, which is a new method of radiative insulation that surrounds VTC-supported SPs with nested (spacerless) boxes of double aluminized Mylar (DAM) that rest on the VTCs; **(4) low conductance thermal isolators (LCTI)**, which are 3D-printable polymer isolators with extremely low conductance; **(5) reverse-operation DTE thermal switch (ROD-TSW)**, which is a new high-performance passive thermal switch with a 2500:1 ON/OFF ratio; **(6) extended stroke ROD-TSW (ES-ROD-TSW)**, which uses two stages and negative CTE Allvar to extend ROD-TSW stroke by 10X to nearly 1 mm for non-vacuum applications while still providing a 13000:1 ON/OFF ratio in vacuum; **(7) miniaturized ROD-TSW (mini-ROD-TSW)**, which uses four reduced-length stages to create a compact (35 mm D, H), lightweight (30 g) ROD-TSW that is projected to have a 1000:1 ON/OFF ratio, although it has not yet been performance tested; **(8) miniaturized loop heat pipes (mini-LHP)**, which provide thermal acquisition, thermal transport, ultra-high ON/OFF ratio thermal switching, and high effectiveness radiators (because of the intrinsic heat spreading capability of the mini-LHP condenser) in a highly compact package; **(9) Vectran tension cables (VTC)**, which provide SP structural support, conductive isolation, and are an integral part of spacerless MLI; and **(10) wire heat leak minimization (WHLM)** techniques, which are methods to reduce (minimize) the heat leak from TSE wiring.



**Figure 3.** Thermal toolbox elements for extreme environments.

## METHODS

The analytical methods used to assess thermal tool performance during the design process is addressed in this section. The relevant key performance parameters (KPPs) are listed in Table 1. The section is organized into 10 subsections, which describe the associated analytical methods.

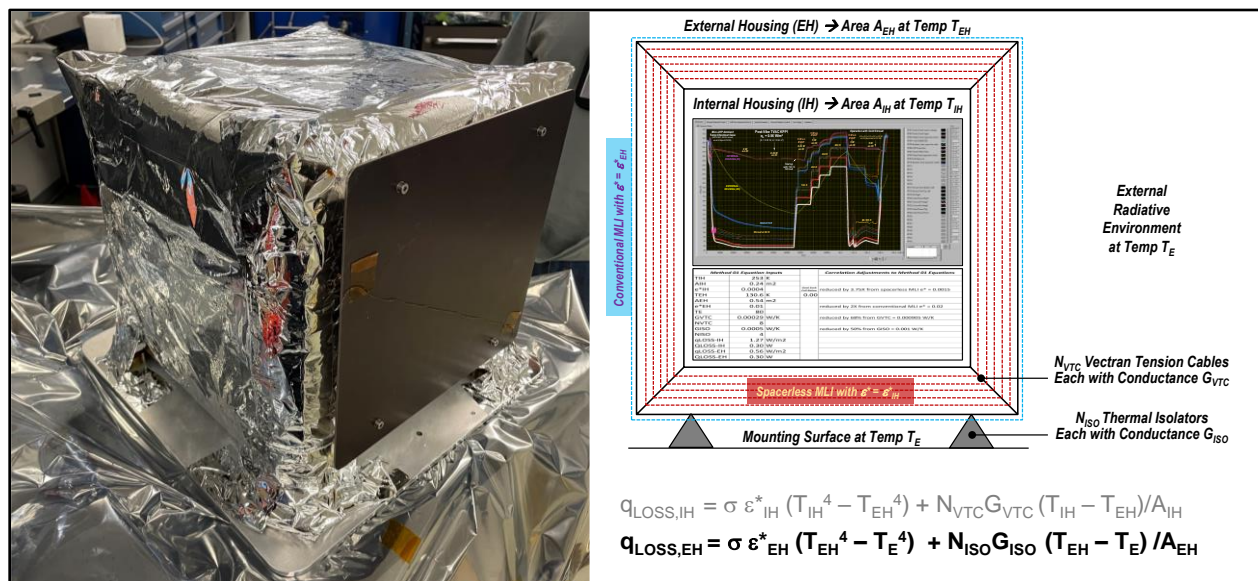
**Table 1.** Key Performance Parameters (KPPs) Used in the Design of Thermal Toolbox Elements

<b>Thermal Tool</b>	<b>Key Performance Parameter (KPP)</b>	<b>Symbol (Units)</b>
1. TSE	Lunar night heat loss flux	$q_{LOSS}$ (W/m <sup>2</sup> )
2. PRR	Lunar surface radiative sink temperature	$T_s$ (K)
3. SMLI	Effective emissivity	$\epsilon^*$
4. LCTI	Thermal conductance	$G$ (W/K)
5. ROD-TSW	Thermal conductance (ON, ON-OFF transition, OFF)	$G$ (W/K)
6. ES-ROD-TSW	Thermal conductance (ON, ON-OFF transition, OFF)	$G$ (W/K)
7. mini-ROD-TSW	Thermal conductance (ON, ON-OFF transition, OFF)	$G$ (W/K)
8. mini-LHP	Thermal conductance (OFF)	$G_{OFF}$ (W/K)
9. VTC	VTC-supported structure spring constant, frequency	$k$ (N/m), $\nu$ (Hz)
10. WHLM	Optimum arrangement for reducing wiring heat leak	$Q_{OPT}$ (W)

### 1. TSE Lunar Night Heat Loss Flux ( $q_{LOSS}$ )

The TSE lunar night heat loss flux ( $q_{LOSS}$ ) is the heater power ( $Q_H$ ) needed to keep the TSE internal housing (IH) above 253 K during lunar night divided by the TSE external housing (EH) area ( $A_{EH}$ ). Equation 1 indicates that  $q_{LOSS}$  includes radiative and conductive heat loss terms. On the NASA GCD-funded PALETTE project, developing a TSE that would reduce  $q_{LOSS}$  to 3 W/m<sup>2</sup> (or lower) was the project goal. The actual  $q_{LOSS}$  value attained during PALETTE was 0.56 W/m<sup>2</sup>. Figure 4 illustrates the situation. The two boxed graphics within the IH envelope are the PALETTE Task 1 Test 1B test data (top box) and  $q_{LOSS}$  spreadsheet computational tool (bottom box). The information contained within top box demonstrates how effective the TSE is at minimizing  $q_{LOSS}$ . To match the Task 1 Test 1B test data, several parameters in the spreadsheet (bottom box) were reduced, indicating the TSE actually performs better than predicted.

$$q_{LOSS} = \sigma \epsilon^*_{EH} (T_{EH}^4 - T_E^4) + N_{ISO} G_{ISO} (T_{EH} - T_E) / A_{EH} \quad (1)$$



**Figure 4.** TSE lunar night heat loss flux ( $q_{LOSS}$ ) analytical methods.

## 2. PRR Lunar Surface Radiative Sink Temperature ( $T_S$ )

The PRR lunar surface radiative sink temperature ( $T_S$ ) is the temperature attained by a side-facing radiator of a science payload (SP) at lunar noon with no SP power dissipation and it is computed using the procedure and equations outlined in Figure 5. Also shown in Figure 5 is the PALETTE Task 2 Prototype PRR and three small boxed items that illustrate (from left to right) PRR rationale, LuSEE-Night preliminary PRR thermal balance, and PALETTE Task 2 test data (note: surrounding the test data box is a larger box showing a correlated Excel spreadsheet model implementing the equations shown in the figure). Equation 2 is the analytical tool needed to compute  $T_S$ . The  $T_S$  goal on PALETTE was 215 K. However, during testing, a  $T_S$  value of 231 K was obtained, which could have been 5-10 K lower by taking extra build/integration steps that: (a) maximize reflectance (R) from PRR frontal area by covering open gaps or high  $\epsilon$  areas with double aluminized Mylar; and (b) minimize heat leaks ( $\sum_i Q_i$ ) into the PRR. On a flight PRR attached to a TSE-housed SP, heat leaks into the PRR emanate from environment/lander/TSE. Heat leaks into the TSE from the environment/lander should also be minimized since that heat leak is also serviced by the PRR.

$$T_S = [\sum_i Q_i / (\eta_R \epsilon_R A_R \sigma)]^{0.25} \quad (2)$$

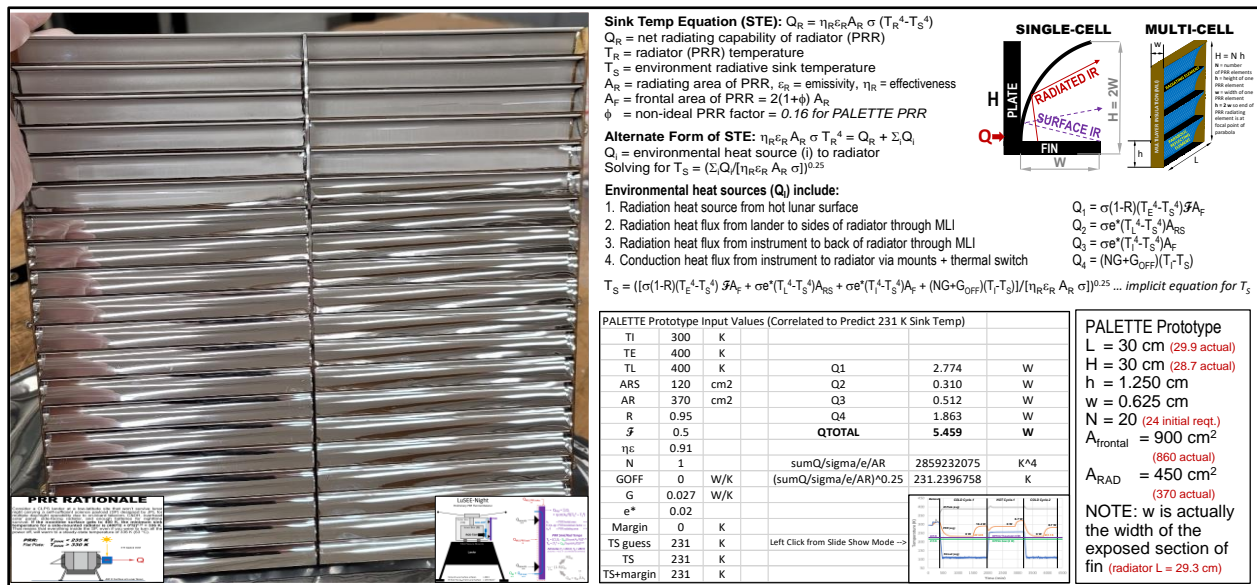


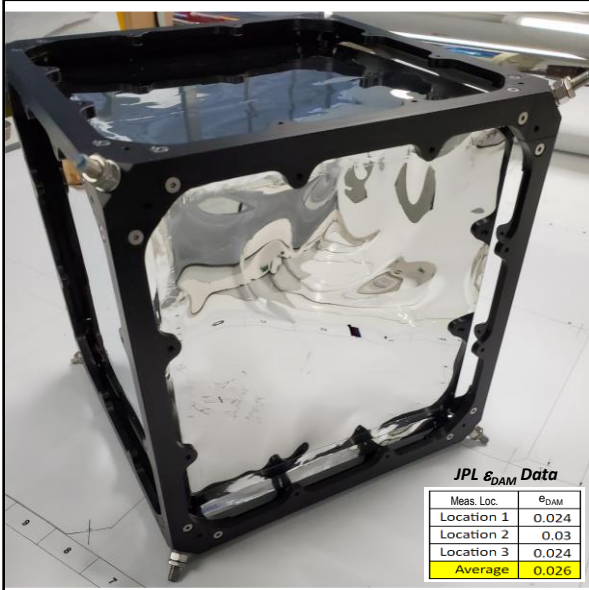
Figure 5. PRR lunar surface radiative sink temperature ( $T_S$ ) analytical methods.

## 3. SMLI Effective Emissivity ( $\epsilon^*$ )

Effective emissivity is defined as the radiative heat flux ( $q_{H-to-C}$ ) transferred from surface H (at  $T_H$ ) to surface C (at  $T_C$ ) divided by  $\sigma(T_H^4 - T_C^4)$ . The parameter  $\epsilon^*$  can also be thought of as the radiative coupling per unit area ( $G_R/A$ ) between those surfaces. For infinite parallel planar surfaces, with emissivity values  $\epsilon_H$  and  $\epsilon_C$ , respectively,  $\epsilon^* = G_R/A = 1/(1/\epsilon_H + 1/\epsilon_C - 1)$ . Now, if we attempt to reduce the radiative heat transfer rate by adding N double aluminized Mylar (DAM) layers between surfaces H and C,  $\epsilon^*$  can be estimated by using Equation 3.

$$\epsilon^* = 1/[2(1/\epsilon_{H/C} + 1/\epsilon_{DAM} - 1) + (N - 1)(2/\epsilon_{DAM} - 1)] \quad (3)$$

The derivation of Equation 3 is based on the fact that if we place N DAM layers between surfaces H and C, there will be N+1 (Surface A-to-Surface B) radiative couplings per unit area in series, each given by  $[G_R/A]_{A-B} = 1/(1/\epsilon_A + 1/\epsilon_B - 1)$ . That total of N+1 is composed of N-1 DAM-to-DAM couplings, where  $[G_R/A]_{DAM-to-DAM} = (N-1)(2/\epsilon_{DAM} - 1)$ , in series with 1 H-to-DAM coupling, where  $[G_R/A]_{H-to-DAM} = (1/\epsilon_H + 1/\epsilon_{DAM} - 1)$ , in series with 1 C-to-DAM coupling, where  $[G_R/A]_{C-to-DAM} = (1/\epsilon_C + 1/\epsilon_{DAM} - 1)$ . By combining  $[G_R/A]_{DAM-to-DAM}$ ,  $[G_R/A]_{H-to-DAM}$ , and  $[G_R/A]_{C-to-DAM}$  in series (where we assume  $\epsilon_H = \epsilon_C = \epsilon_{H/C}$ ), one arrives at Equation 3. And based on that equation, very low  $\epsilon^*$  values are possible with just a few layers. In practice, due to seams, folds, and spacers (SFS), conventional MLI  $\epsilon^*$  values are rarely less than 0.02. Spacerless MLI (SMLI) eliminates SFS by hanging nested DAM layers on VTC supports and, as Figure 6 shows, has a measured  $\epsilon^* = 0.0015$ . Equation 3 with  $N = 8$ ,  $\epsilon_{H/C} = 0.9$  ( $\epsilon_{H/C} = \epsilon_{CUBE}$  in Figure 6), and  $\epsilon_{DAM} = 0.026$ , yields an  $\epsilon^* = 0.0016$ .



The PALETTE Spacerless MLI (SMLI) test unit consisted of an internal cube ( $\epsilon = \epsilon_{CUBE}$ ), 8 spacerless layers of double aluminized Mylar or DAM ( $\epsilon = \epsilon_{DAM}$ ), and an external cube ( $\epsilon = \epsilon_{CUBE}$ ). For this system, the  $\epsilon^*$  for N parallel plates (*ignoring variable area effect*) is ...

$$\epsilon^* = 1/[2(1/\epsilon_{CUBE} + 1/\epsilon_{DAM} - 1) + (N - 1)(2/\epsilon_{DAM} - 1)]$$


**note:** if  $\epsilon_{CUBE} = \epsilon_{DAM}$ ,  $\epsilon^* = 1/[(N+1)(2/\epsilon_{DAM} - 1)]$

JPL measurements of DAM emissivity indicated  $\epsilon_{DAM} = 0.026$ .


Plugging in  $\epsilon_{DAM} = 0.026$ ,  $\epsilon_{CUBE} = 0.9$ ,  $N = 8$  into above equation yields  $\epsilon^* = 0.0016$ .

Drawings, photos, and test data for PALETTE spacerless MLI are shown below. **Measured  $\epsilon^* = 0.0015$ .** Use maximum magnification to see content in the three boxes below.

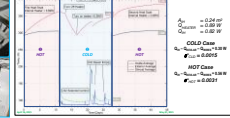
**Drawing**



**Photos**



**Test Data**



Mess. Loc.	$\epsilon_{DAM}$
Location 1	0.024
Location 2	0.03
Location 3	0.024
<b>Average</b>	<b>0.026</b>

Thus, it appears (at least for the cold case) that Spacerless MLI performs very similarly to multiple parallel low emissivity plates.

**Figure 6.** SMLI effective emissivity ( $\epsilon^*$ ) analytical methods.

#### 4. LCTI Thermal Conductance (G)

The LCTI thermal conductance (G), while easy to compute analytically with Thermal Desktop (TD), is quite difficult to validate by TVAC test measurement because G is so low. The analytical method used to measure LCTI G in TVAC testing is illustrated in Figure 7. The method utilizes a 0.1 W/K Q-meter (QM) and a QM Calibration (QMC) process known as “in-situ calibration”. Equation 4 depicts the analytical relationship (*note:  $\Delta T$  values in Equation 4 will be defined shortly*).

$$G = (\Delta T_{QMT}/\Delta T_{QMC}) Q_{QMC} / \Delta T_p \quad (4)$$

The method involves setting up the system as illustrated in Figure 7 by first bolting disc-shaped aluminum “pucks” to the LCTI top (green puck) and LCTI bottom (red puck). The red puck is bolted to the QM top, the QM bottom is bolted to a cooling source (which holds the QM bottom at a

constant temperature), a heater (H1) is attached to the QM bottom, another heater (H2) is attached to the red puck (QM top), and a third heater (H3) is attached to green puck (LCTI top).

After setting up the system as described above (and surrounding the assembly with a single DAM cylinder), a LCTI conductance test is carried out as follows. First, the cooling source is turned on and the QM bottom, with H1 set to 0.5 W, cools the entire setup so that the QM bottom reaches a desired temperature and is held there while the rest of the system cools. When the QM bottom is steady, the QM top heater H2 is set to 0.5 W and the QM bottom heater H1 is turned off. This is the QM Calibration (QMC) step. The QM top then rises  $\Delta T_{QMC}$  above QM bottom. Next, H2 is set to 0 W, H1 is set back to 0.5 W, and H3 is turned on at about 0.2 W. This step causes the green puck to rise appreciably by  $\Delta T_P$  while the red puck rises by only  $\Delta T_{QMT}$ . Heat flow through the LCTI ( $Q_{LCTI}$ ) is assumed equal to  $([\Delta T_{QMT}/\Delta T_{QMC}]Q_{QMC})$ , hence  $G_{LCTI} = Q_{LCTI}/\Delta T_P$ , as Equation 4 indicates.

As mentioned at the top of Figure 7, PALETTE LCTIs were made from 3 different materials (machinable Ultem 1000 and 3D-printable Ultem 9085/1010) in two sizes (short, tall). Thus, six total configurations were TVAC tested and 2 or 3 such tests of each configuration were carried out. Figure 7 also provides views of the five LCTI concepts, TD modeling results, TVAC test results, and a tensegrity LCTI prototype (which was also tested using this method, but not as part of PALETTE). Use of document zoom to discern some Figure 7 content may be required.

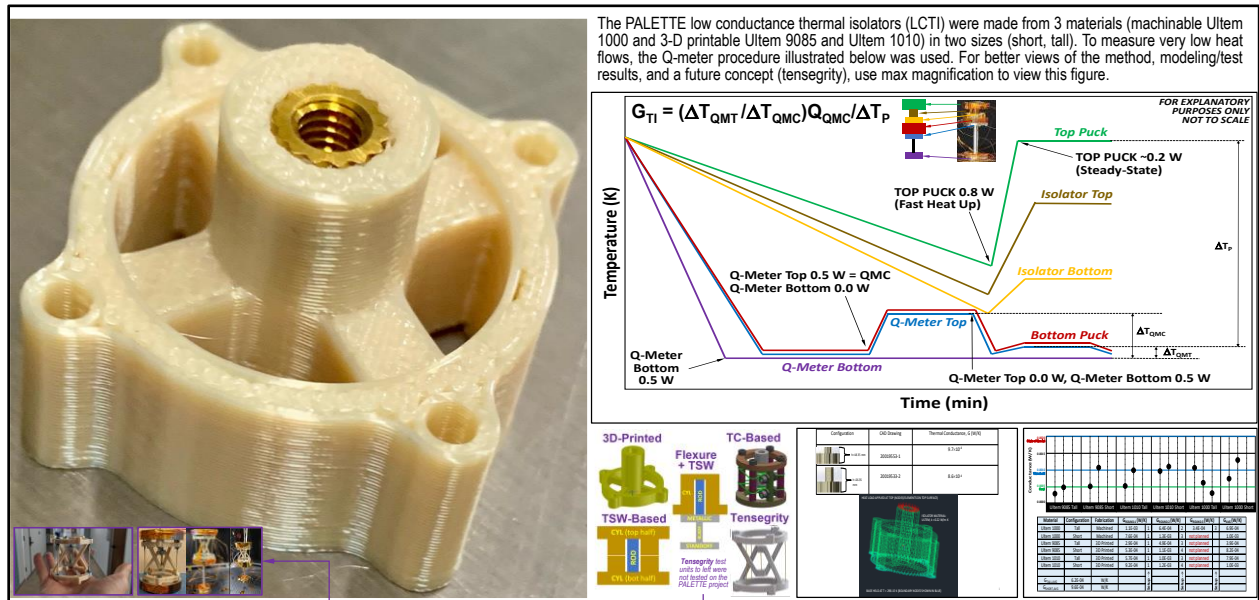


Figure 7. LCTI thermal conductance (G) analytical methods.

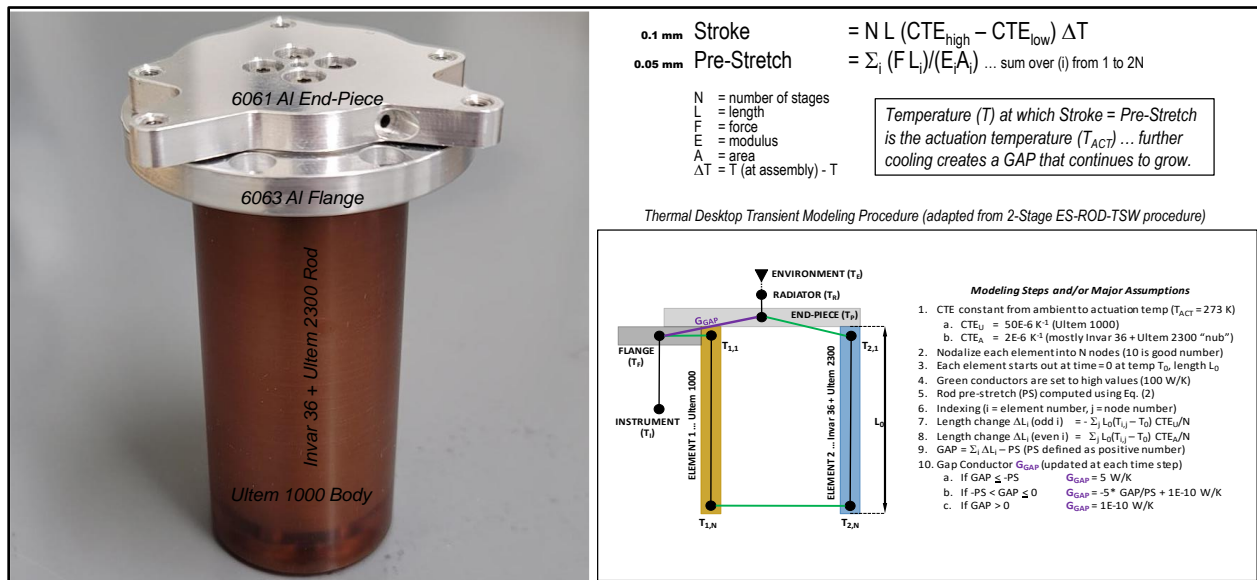
### 5. ROD-TSW Thermal Conductance ON/OFF ( $G_{ON}$ , $G_{OFF}$ )

The ROD-TSW is a passive thermal switch that modulates heat flow (from fully ON to fully OFF) via **single-stage** DTE between a high CTE body (either Ultem 1000 or 6061 Al) and a low CTE rod (Invar 36 with a small Ultem 2300 “nub”). Figure 8 illustrates the Ultem 1000 body version. The figure also provides the two essential governing equations and an algorithm for actively modeling ROD-TSW transient thermal performance in Thermal Desktop (TD). A ROD-TSW identical to the

one pictured in Figure 8 is slated to be flown on the Farside Seismic Suite (FSS) mission to Schrodinger Basin on the lunar farside sometime in 2025. In TVAC performance testing at JPL in 2018, two ROD-TSW prototypes (Ultem 1000 and 6061 Al body versions) both exhibited ON/OFF ratios of roughly 2500:1 ( $G_{ON} = 5 \text{ W/K}$ ,  $G_{OFF} = 0.002 \text{ W/K}$ ). The ON/OFF temperature of actuation is typically 273 K but can be raised or lowered by 5-10 K by reducing or increasing the pre-stretch (PS). The governing equations for stroke (S) and pre-stretch (PS) are provided below as Equations 5 and 6 (**note:** N = number of stages, L = characteristic length,  $CTE_{high}$  = CTE of high CTE material,  $CTE_{low}$  = CTE of low CTE material,  $\Delta T$  = temperature difference over which ON/OFF performance is calculated, F = desired PS force, E = modulus of elasticity, and A = cross-sectional area).

$$S = N L (CTE_{high} - CTE_{low}) \Delta T \tag{5}$$

$$PS = \sum_i (F L_i) / (E_i A_i) \dots \text{sum over } (i) \text{ from } i = 1 \text{ to } N \tag{6}$$



**Figure 8.** ROD-TSW ON/OFF behavior analytical methods.

### 6. ES-ROD-TSW Thermal Conductance ON/OFF ( $G_{ON}$ , $G_{OFF}$ )

The ES-ROD-TSW is a passive thermal switch that modulates heat flow (from fully ON to fully OFF) via **dual-stage** DTE between a high CTE body/nested cylinder (Ultem 1000) and a low CTE nested cylinder/rod (Invar 36). Figure 9 illustrates the ES-ROD-TSW prototype. The figure also provides the two essential governing equations and provides an algorithm for actively modeling ES-ROD-TSW transient thermal performance in Thermal Desktop (TD). With a stroke approaching 1 mm, which is 10X that of the original ROD-TSW, the ES-ROD-TSW (while primarily intended for non-vacuum applications), has exhibited an ON/OFF ratio in vacuum of 13000:1 in TVAC testing at JPL.

The ES-ROD-TSW in-vacuum ON/OFF ratio indicated above was attained with a measured ON conductance ( $G_{ON}$ ) of 6.5 W/K and a calculated OFF conductance ( $G_{OFF}$ ) of 5E-4 W/K, which yields the 13000:1 ratio. The rationale for using the calculated (not the measured)  $G_{OFF}$  value is that the test did not use a QM, thus the ultra-low heat flows (in the OFF state) could not be measured.



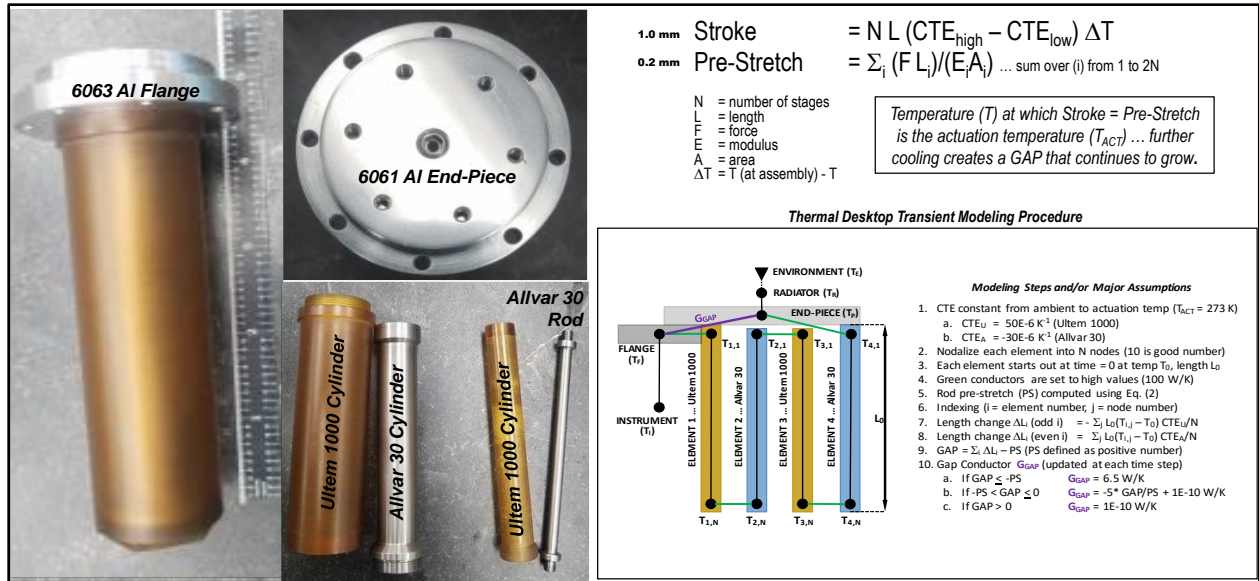


Figure 9. ES-ROD-TSW ON/OFF behavior analytical methods.

7. mini-ROD-TSW Thermal Conductance ON/OFF ( $G_{ON}$ ,  $G_{OFF}$ )

The mini-ROD-TSW is a totally passive thermal switch that modulates heat flow (from fully ON to fully OFF) via **quad-stage** DTE between a high CTE body and cylinders (6061 Aluminum) and low CTE cylinders and rod (Invar 36). Figure 10 illustrates the initial prototype. The figure also lists the two essential governing equations and provides an algorithm for actively modeling its transient thermal performance in Thermal Desktop (TD). The mini-ROD-TSW has yet to be TVAC performance tested, but it is projected to have an ON/OFF ratio of 1000:1 ( $G_{ON} = 2 \text{ W/K}$ ,  $G_{OFF} = 0.002 \text{ W/K}$ ). Shown at the lower left of Figure 10 is a small graphic illustrating the various parts within the mini-ROD-TSW (*note*: document zoom may be required to discern this content).

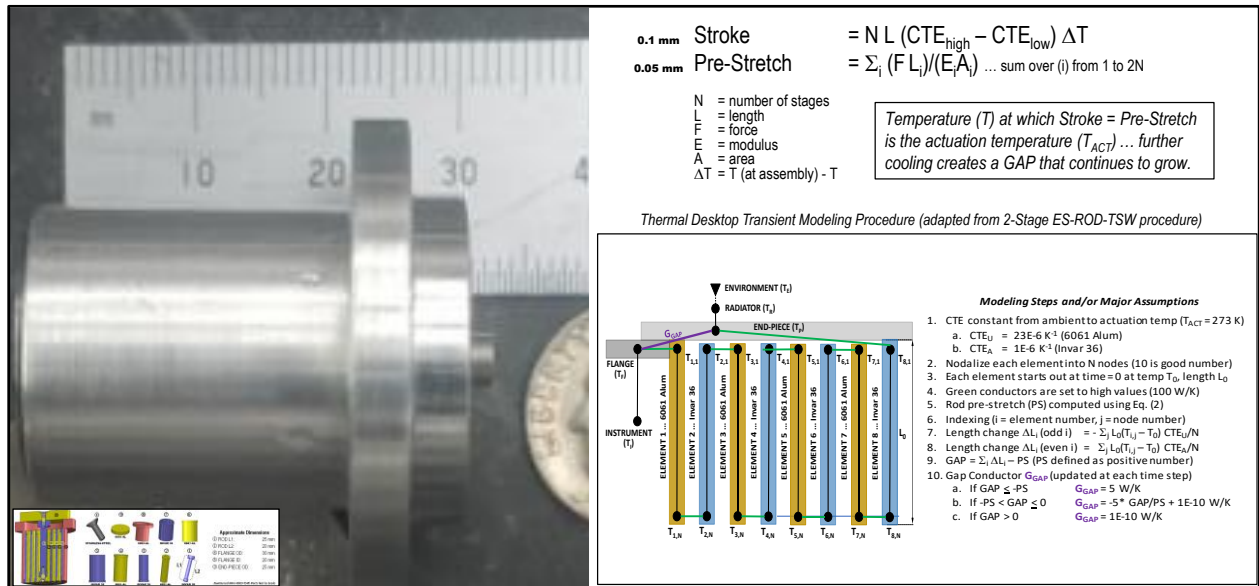
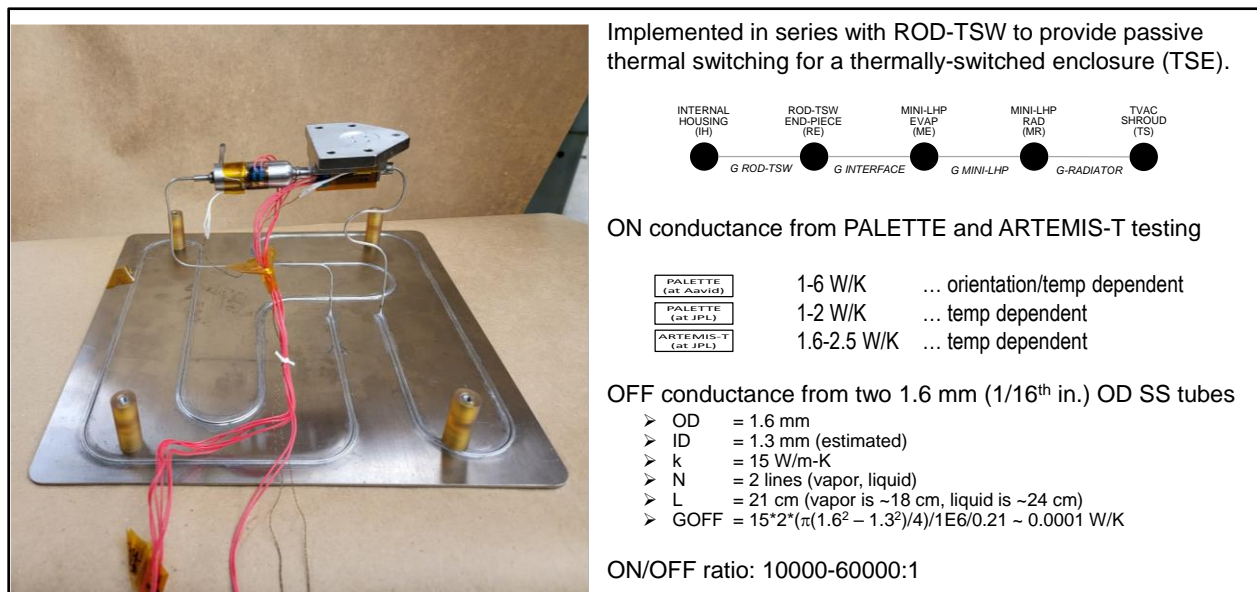


Figure 10. Mini-ROD-TSW ON/OFF behavior analytical methods.

## 8. mini-LHP Thermal Conductance OFF ( $G_{OFF}$ )

The mini-LHP is a (nearly) fully passive device that provides thermal acquisition, transport, switching, and radiator heat spreading. It is not fully passive because a startup heater is sometimes needed to start circulation and a shutdown heater is sometimes needed to end circulation. During the PALETTE project, a mini-LHP was paired in series with a ROD-TSW. The goal was to eliminate the need for mini-LHP startup/shutdown heaters. While PALETTE testing has shown that a startup heater is still required, the ROD-TSW does eliminate the need for a shutdown heater. Interestingly, when the ROD-TSW and mini-LHP are paired in series and both are OFF, the system OFF conductance is dominated by the mini-LHP, as described below.

Mini-LHP ON conductance is difficult to predict analytically, thus it must be measured by testing. However, mini-LHP OFF conductance can be readily calculated. Figure 11 provides OFF conductance calculations as well as ON conductance values obtained during PALETTE and ARTEMIS TSE testing, which was carried out with a ROD-TSW in series with a propylene mini-LHP. As indicated in the figure, mini-LHP OFF conductance ( $G_{OFF}$ ) is predicted to have the exceedingly low value of just 0.0001 W/K, which outperforms the ROD-TSW in OFF conductance by a factor of 50. Depending on which ON conductance test measurements are used (PALETTE at Aavid, PALETTE at JPL, or ARTEMIS-T at JPL), the mini-LHP ON/OFF ratio is in the range of 10000-60000:1.



**Figure 11.** Mini-LHP OFF conductance analytical methods.

## 9. VTC Spring Constant (k) and Frequency ( $\nu$ )

To minimize conductive/radiative heat loss from TSEs, VTC-supported structures (IH cube frame within EH cube frame) are used. All temperature sensitive elements are housed within the IH, which is supported from the EH by 8 corner VTCs. To facilitate early design trades, a simple analytical method was needed to calculate the (translation/rotational) first mode frequencies. Figure 12 depicts the model equations and spreadsheet model results for FSS. As indicated, the frequencies predicted by this simple model agree with those predicted by the FSS flight FEM.

Two of the key quantities that go into the translational and rotational frequencies are the cable axial and lateral stiffnesses or spring constants ( $k$ ), which are presented below as Equations (7) and (8). As indicated in Equation (7), the effective modulus ( $E_{EFF}$ ) of these VTCs (which are Vectran ropes epoxied into threaded end-fittings) at 22 GPa is quite a bit lower than the modulus of pure Vectran ( $E_{Vectran}$ ), which is 50-100 GPa depending on the type of Vectran.

$$AS = k_s = E_{EFF} A / L \dots \text{where } E_{EFF} = 22 \text{ GPa} \ll E_{Vectran} \quad (7)$$

$$LS = k_L = F/L \quad (8)$$

To determine the first-mode frequencies ( $\nu$ ) of the IH, which is supported by 8 VTCs, refer to the last four of six equations at the lower left of Figure 12. Also shown in Figure 12 are five boxed items with small graphics that probably require document zoom. These items, from left to right on the figure, are: (1) the VTC sizing spreadsheet, created by Richard Bahng, a JPL structural engineer; (2) pull test results for the FSS 6.35 mm OD VTCs; (3) spacerless MLI Kevlar tension cable (KTC) test article (*note*: KTCs built by JPL did not have sufficient strength and were replaced by VTCs built by Applied Fiber [AF]); (4) AF drawing of a 3.175 mm OD VTC used by PALETTE; and (5) AF drawing of a 6.35 mm OD VTC used by FSS. The photo in Figure 12 shows the FSS prototype being assembled for a TVAC-vibe test sequence, which were both successfully completed.

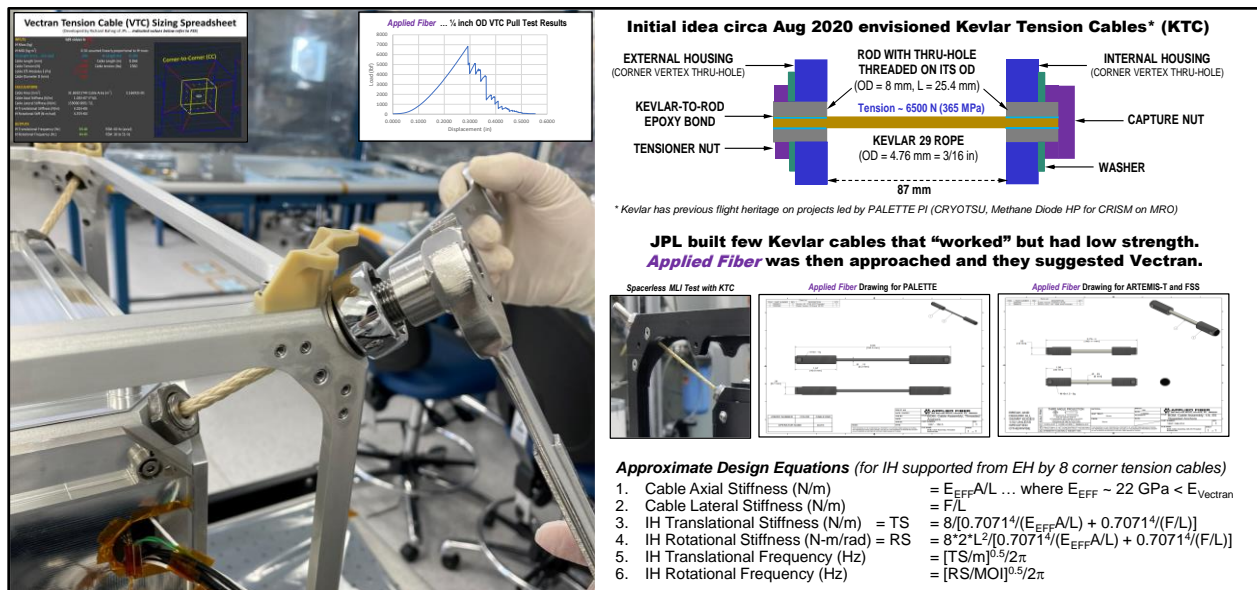


Figure 12. VTC-supported structure translational/rotational frequency analytical methods.

### 10. WHLM Optimum Heat Loss ( $Q_{L,OPT}$ )

To minimize the heat leak from IH-to-EH Cu wiring, there are 3 options: (W1) splice-in phosphor bronze wires but maintain Cu wire resistivity; (W2) route the Cu wires out along a long diagonal path; and (W3) provide a length inside the IH with radiative isolation and a length outside the EH with radiative isolation before heat sinking the wires. All options need to improve on (W0), which is to heat sink the Cu wires to the IH, EH. Combining W1-W3 yields 4 more options (W4a-W4d).

To limit analytical scope, a sample configuration was assumed involving fifty 30-gauge Cu wires that pass from a 30 cm cube IH at 300 K to a 40 cm cube EH at 100 K. The heat leak results for all eight configurations (W0-W3, W4a-W4d) are illustrated in Figure 13. Those results indicate that the lowest heat leak solution is W4d, which is a W1 + W2 + W3 combination. But W4d is not the optimum solution. The optimum solution is the one that best meets all performance criteria including heat leak, simplicity, cost, mass, and others. To determine the optimum solution, the PALETTE project conducted a study with a total of 10 performance criteria and each solution was numerically ranked based on those criteria. In the end, W3 ranked highest. Interestingly, FSS selected W3 as its WHLM architecture before this study was completed, as their principle selection criterion was integration simplicity. Included in Figure 13 is a photo of the FSS prototype test article, which illustrates the external radiative isolation used in the W3 architecture.

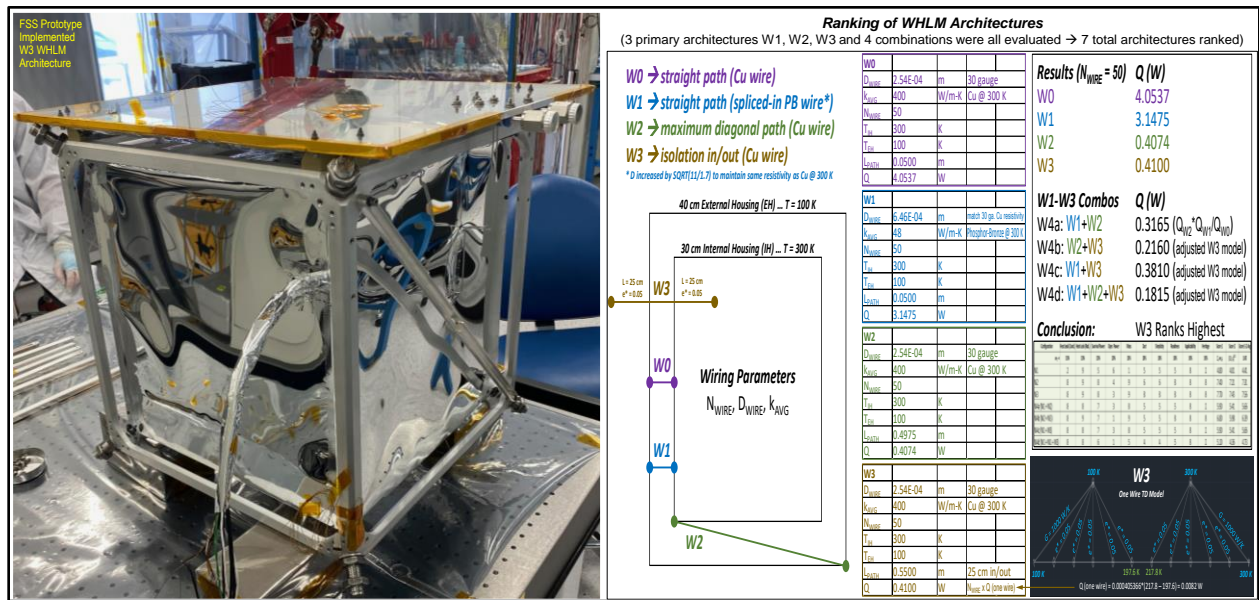
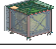

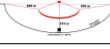
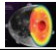



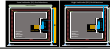

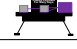


Figure 13. WHLM optimum heat loss determination analytical methods.

## INFUSION

The ultimate goal of all thermal technology development projects is mission infusion and the new thermal toolbox elements described in this paper are well on their way in that regard. Two manifested missions that will utilize these tools, as previously mentioned herein, are FSS and LuSEE-Night. But there are several other possibilities as indicated in Figure 14. Those future possibilities include LCRT<sup>14</sup> (Lunar Crater Radio Telescope), LGN<sup>15</sup> (Lunar Geophysical Network), LVHM<sup>16</sup> (Lunar Vector Helium Magnetometer), LTV<sup>17</sup> (Lunar Terrain Vehicle), VIPER<sup>18</sup> (Volatiles Investigating Polar Exploration Rover), and arbitrary instruments/rovers/landers that seek extended-life operability. Figure 14 was taken directly from a PowerPoint presentation and the boxed items on the left are actually embedded objects with additional information on each application. The TFAWS presentation that accompanies this paper may have time to open a few of those embedded PowerPoint objects to see the key details associated with each manifested or possible mission/system.

<b>FSS</b> <small>Farside Seismic Suite</small>	Manifested Mission	<b>Landing Site:</b> Schrodinger Basin 71° S, Farside <b>Power Dissipation:</b> Day 10 W (25 W during transmit), Night 5 W		<b>Toolbox Features</b> TSE, VTC, SMLI
<b>LuSEE-Night</b> <small>Lunar Surface Electromagnetic Experiment</small>	Manifested Mission	<b>Landing Site:</b> Mid-Latitude, Farside <b>Power Dissipation:</b> Day 25 W (40 W during transmit), Night 12 W		<b>Toolbox Features</b> 2 mini-LHP TSE, PRR
<b>LCRT</b> <small>Lunar Crater Radio Telescope</small>	Possible Mission	<b>Landing Site:</b> Low Latitude (10° S to 10° N), Farside <b>Power Dissipation:</b> Day 165 W, Night 45 W		<b>Toolbox Features</b> TSE, VTC, SMLI, PRR
<b>LGN</b> <small>Lunar Geophysics Network</small>	Possible Mission	<b>Landing Sites:</b> PKT 20.7°, Crisium 18.5°, Schickard -44.3°, Korolev -2.4° <b>Power Dissipation:</b> Day 160 W, Night 40 W (TBR)		<b>Toolbox Features</b> TSE, VTC, SMLI, PRR
<b>LVHM</b> <small>Lunar Vector Helium Magnetometer</small>	Possible Mission	<b>Landing Site:</b> Not selected <b>Power Dissipation:</b> Day 10 W (25 W during transmit), Night 5 W		<b>Toolbox Features</b> TSE, VTC, SMLI, PRR
<b>LTV</b> <small>Lunar Terrain Vehicle</small>	Possible Mission	<b>Landing Site:</b> Lunar South Pole <b>Power Dissipation:</b> Day TBD, Night 50 W minimum (for SPs)		<b>Toolbox Features</b> TSE, VTC, SMLI
<b>VIPER</b> <small>Venus Investigating Polar Exploration Rover</small>	Manifested Mission	<b>Landing Site:</b> Nobile Crater (-85°), Nearside <b>Power Dissipation:</b> Day ~400 W, Night 60-90 W (50 hours)		<b>Toolbox Features</b> TSE with LHPs/TCVs
<b>Instrument</b> <small>Extended Duration Operation/Survival</small>	Possible System	<b>Landing Site:</b> Arbitrary (HL or LL, NS or FS) <b>Power (Typical):</b> Day 5-80 W, Night 0-20 W		<b>Toolbox Features</b> TSE, VTC, SMLI, PRR
<b>Rover</b> <small>Extended Duration Operation/Survival</small>	Possible System	<b>Landing Site:</b> Arbitrary <b>Power (Notional):</b> Day 1-500 W, Night 0-50 W		<b>Toolbox Features</b> TSE, VTC, SMLI, PRR
<b>Lander</b> <small>Extended Duration Operation/Survival</small>	Possible System	<b>Landing Site:</b> Arbitrary <b>Power (Notional):</b> Day 1-1000 W, Night 0-100 W		<b>Toolbox Features</b> TSE, VTC, SMLI, PRR

**Figure 14.** Infusion plans/opportunities for PALETTE, ARTEMIS, and ROD-TSW thermal tools.

## CONCLUSIONS

This paper has presented a set of analytical methods to go along with a new series of thermal toolbox elements for thermally managing science payloads in extreme environments. This set of analytical methods enables the hand calculation, numerical simulation, and/or test measurement of: (a) lunar night heat loss flux ( $q_{\text{Loss}}$ ) of thermally-switched enclosures (TSE); (b) lunar noon radiative sink temperature ( $T_s$ ) for parabolic reflector radiators (PRR); (c) effective emissivity ( $\epsilon^*$ ) of spacerless multilayer insulation (SMLI); (d) thermal conductance ( $G$ ) of low conductance thermal isolators (LCTI); (e) ON/OFF behavior of reverse-operation DTE thermal switches (ROD-TSW, ES-ROD-TSW, mini-ROD-TSW) and miniaturized loop heat pipes (mini-LHP); (f) spring constant ( $k$ ) and frequency ( $\nu$ ) of Vectran tension cable (VTC) supported structures; and (g) optimized heat leak ( $Q_{\text{OPT}}$ ) of wire heat leak minimization (WHLM) techniques. This new set of thermal tools and methods has already been applied to the currently manifested FSS, LuSEE-Night, and VIPER missions and may eventually be infused into several future mission possibilities including LCRT, LGN, LTV and others.

## ACKNOWLEDGEMENTS

The authors would like to acknowledge the significant contributions of the personnel and suppliers listed in Figure 15 to the work described herein. Although that figure was specifically prepared for the NASA GCD sponsored PALETTE project, many (if not most) listed there also contributed to the ARTEMIS, ROD-TSW, ES-ROD-TSW and mini-ROD-TSW projects. This research was carried out at the Jet Propulsion Laboratory, California Institute of Technology, under a contract with the National Aeronautics and Space Administration (80NM0018D0004).

<b>Key Contributors to PALETTE (JPL)</b>	
<ul style="list-style-type: none"> <li>• Jose Rivera</li> <li>• John Elliott</li> <li>• Eric Sunada</li> <li>• Pamela Clark</li> <li>• Tim O'Donnell</li> <li>• Doug Hofmann</li> <li>• Garry Burdick</li> <li>• Sabrina Feldman</li> <li>• Ying Lin</li> <li>• Satish Khanna</li> <li>• David Eisenman</li> <li>• Andrew Gray</li> <li>• Virgil Mireles</li> <li>• Gani Ganapathi</li> <li>• Chuck Phillips</li> </ul>	<p>Agreed to help run several tech-dev projects (ARTEMIS-T, Astrobotic, ES-ROD-TSW, FSS Proposal, etc.)</p> <p>Suggested need for thermal switch for Lunette and defined need for parabolic reflector radiator (PRR)</p> <p>Encouraged development of Reverse-Operation DTE Thermal Switch (ROD-TSW)</p> <p>Suggested need for thermal switch for lunar night survival of SILVIR IR spectrometer concept</p> <p>Helped with Spontaneous R&amp;TD Proposal for ROD-TSW and provided great advice on all projects</p> <p>Helped with Spontaneous R&amp;TD Project for ROD-TSW, CIF Advanced Concepts ES-ROD-TSW project</p> <p>Provided internal JPL funding for ROD-TSW qual. testing, suggested CLPS lander independence (retired)</p> <p>Provided internal JPL funding for ROD-TSW qual. testing, initiated ARTEMIS project w/D. Bugby as lead</p> <p>ARTEMIS-T SR&amp;TD initiative lead has provided great guidance throughout</p> <p>Provided great strategic direction to ARTEMIS-T and indirectly to PALETTE</p> <p>Program manager for Lunar CATALYST which funded ROD-TSW thermal switching system for Astrobotic</p> <p>JPL Program Office interface to NASA GCD</p>
<b>PALETTE Team Members (JPL)</b>	
<ul style="list-style-type: none"> <li>• David Bugby</li> <li>• Jose Rivera</li> <li>• Doug Hofmann</li> <li>• Pamela Clark</li> <li>• Scott Roberts</li> <li>• Stefano Morellina</li> <li>• Bob Kovac</li> <li>• Bart Patel</li> <li>• Kurt Gonter</li> <li>• Jason Kempenaar</li> <li>• Kevin Anderson</li> <li>• Richard Bahng</li> <li>• Chris Chrzanowski</li> <li>• Kris Stone</li> <li>• Joanna Farias</li> </ul>	<p>PI, Technical/Management</p> <p>Co-I, Technical/Management</p> <p>Co-I, Advanced Materials</p> <p>Co-I, Lunar Science (left JPL)</p> <p>Additive Manufacturing (AM)</p> <p>Thermal Design, CAD, AM</p> <p>Design, CAD, Fabrication</p> <p>Design, CAD (APR Consulting)</p> <p>Thermal Design/Analysis (left JPL)</p> <p>Thermal Design/Analysis (left JPL)</p> <p>Thermal Analysis</p> <p>Structural Analysis</p> <p>Structural Analysis</p> <p>Testbed Development, Testing</p> <p>Assembly, Fabrication, Testing</p>
<b>Key Suppliers to PALETTE</b>	
<ul style="list-style-type: none"> <li>• Mini-LHP</li> <li>• Graphite Straps</li> <li>• Al Housings</li> <li>• Design/CAD</li> <li>• Tension Cables</li> <li>• Structural Analysis</li> </ul>	<p>Aavid/Thermacore (Boyd Corporation)</p> <p>Thermotive LLC</p> <p>Wirecut Company</p> <p>APR Consulting (Bart Patel)</p> <p>Applied Fiber</p> <p>Quartus Engineering</p>
<b>NASA STMD/GCD Technology Management Team</b>	
<ul style="list-style-type: none"> <li>• Quynhgiao Nguyen</li> <li>• Fred Elliott</li> <li>• Shawn Britton</li> <li>• Amanda Cutright</li> <li>• Mark Thornblom</li> <li>• David Goggin</li> <li>• Jeff Antol</li> <li>• Kevin Somerville</li> <li>• Angela Krenn</li> <li>• Lee Mason</li> <li>• Jeff Sheehy</li> </ul>	<p>Program Element Manager-3, GCD</p> <p>Program Element Manager-2, GCD</p> <p>Program Element Manager-1, GCD</p> <p>Chief Engineer, GCD</p> <p>Deputy Program Manager, GCD</p> <p>Chief Engineer's Office, GCD</p> <p>Chief Engineer's Office, GCD (retired)</p> <p>TIM Extreme Environments, STMD</p> <p>Thermal Principal Technologist, STMD</p> <p>Deputy Chief Engineer, STMD</p> <p>Chief Engineer, STMD</p>

**Figure 15.** Personnel and organizations that contributed mightily to this work.

## APPENDIX

Terms that were not included in the Nomenclature, Acronyms, and Abbreviations section are listed and defined below.

A	Area (m <sup>2</sup> )
A <sub>F</sub>	Frontal Area (m <sup>2</sup> )
A <sub>R</sub>	Radiator Area (m <sup>2</sup> )
D	Diameter (m)
DAM	Double Aluminized Mylar
ΔT	Temperature Difference (K)
E	Modulus of Elasticity (N/m <sup>2</sup> )
E <sub>EFF</sub>	Effective Modulus of Elasticity (N/m <sup>2</sup> )
ε*	Effective Emissivity
EH	External Housing
F	Force (N)
FSS	Farside Seismic Suite
G	Thermal Conductance (W/K)
G <sub>ISO</sub>	Thermal Conductance of Isolators (W/K)
G <sub>OFF</sub>	OFF Thermal Conductance (W/K)
G <sub>ON</sub>	ON Thermal Conductance (W/K)
H	Height (m)
IH	Internal Housing
k	Spring Constant (N/m) or Thermal Conductivity (W/m-K)
KPP	Key Performance Parameter
L	Length (m)
LCRT	Lunar Crater Radio Telescope

LCTI	Low Conductance Thermal Isolator
LGN	Lunar Geophysical Network
LTV	Lunar Terrain Vehicle
LuSEE-Night	Lunar Surface Electromagnetics Experiment-Night
LVHM	Lunar Vector Helium Magnetometer
N <sub>ISO</sub>	Number of Isolators
PRR	Parabolic Reflector Radiator
PS	Pre-Stretch (m)
q <sub>LOSS</sub>	Lunar Night Heat Loss Flux (W/m <sup>2</sup> )
QM	Q-Meter
QMC	QM Calibration
QMT	QM Top
S	Stretch (m)
SFS	Seams, Folds, and Spacers
SMLI	Spacerless Multilayer Insulation
SP	Science Payload
T	Temperature (K)
T <sub>E</sub>	Environment Temperature (K)
T <sub>S</sub>	Sink Temperature (K)
TD	Thermal Desktop
TSE	Thermally-Switched Enclosure
v	Frequency (Hz)
VIPER	Volatiles Investigating Polar Exploration Rover

## CONTACT

### Author e-mail addresses:

D. Bugby [david.c.bugby@jpl.nasa.gov](mailto:david.c.bugby@jpl.nasa.gov)  
 J. Rivera [jose.g.rivera@jpl.nasa.gov](mailto:jose.g.rivera@jpl.nasa.gov)

## REFERENCES

1. Bugby, D. C. Rivera, J. G., and Britton, S. R., "Planetary and Lunar Environment Thermal Toolbox Elements (PALETTE) Project Year One Results," *50<sup>th</sup> International Conference on Environmental Systems*, ICES-2021-409, July 12-15, 2021.
2. Bugby, D. C., Rivera, J. G., and Britton, S. R., "Planetary and Lunar Environment Thermal Toolbox Elements (PALETTE) Project Year Two Results," *51<sup>st</sup> International Conference on Environmental Systems*, ICES-2022-423, July 10-14, 2022.
3. Bugby, D. C., Rivera, J. G., and Nguyen, Q. N., "Planetary and Lunar Environment Thermal Toolbox Elements (PALETTE) Project Final Results," *52<sup>nd</sup> International Conference on Environmental Systems*, ICES-2023-241, July 16-20, 2023.

4. Bugby, D. C., Rivera, J. G., and Lin, Y., "Instrument Thermal Management for Lunar Night Survival without Radioisotopes," *50<sup>th</sup> International Conference on Environmental Systems*, ICES-2021-414, July 12-15, 2021.
5. Bugby, D. C. and Rivera, J. G., "High Performance Thermal Switch for Lunar and Planetary Surface Extreme Environments," *2020 International Conference on Environmental Systems (ICES)*, ICES-2020-145, July 2020.
6. Bugby, D. C., Rivera, J. G., Mauro, S. L., and Farmer, J. T., "Extended Stroke and Miniaturized Reverse-Operation DTE Thermal Switches," *50<sup>th</sup> International Conference on Environmental Systems*, ICES-2021-412, July 12-15, 2021.
7. Panning, M.P, Kedar, S., et. al, "Farside Seismic Suite (FSS): Surviving the Lunar Night and Delivering the First Seismic Data from the Farside of the Moon," *2022 International Planetary Probe Workshop*, Santa Clara, CA, August 29-September 2, 2022.
8. Bale, S. D., Bassett, N., Burns, J. O., Jones, J. D., Goetz, K., et. al, "LuSEE 'Night': The Lunar Surface Electromagnetics Experiment," *URSI GASS 2023*, Sapporo, Japan, August 19-26, 2023.
9. Bugby, D. C. and Rivera, J. G., "Thermal Innovations for Extended-Duration Lunar Operability and Survivability," *Commercial Lunar Payload Services Survive the Night Technology Workshop*, NASA GRC, Cleveland, OH, December 6-8, 2022.
10. Bugby, D. C., Rivera, J. G., and Britton, S. G., "Lunar Night Survivability of Science Payloads Using PALETTE Thermal Technologies," *2022 Spacecraft Thermal Control Workshop*, Virtual Conference, May 24-26, 2022.
11. Bugby, D. C., Rivera, J. G., and Britton, S. G., "Lunar Night Survivability of Cryocooled Instruments Using PALETTE Thermally-Switched Enclosures," *International Cryocooler Conference*, Bethlehem, PA, June 27-30, 2022.
12. Bugby, D. C., "Passive Thermal Management Technologies for Lunar Day/Night Survivability," *Lunar Surface Innovation Consortium, Low Temperature Sub-kW Power and Energy Storage for the Lunar Surface Workshop*, July 28, 2022.
13. Bugby, D. C. and Rivera, J. G., "Lunar Night Survivable Architecture for Self-Sufficient Science Payloads," *2022 International Planetary Probe Workshop*, Santa Clara, CA, August 29 – September 2, 2022.
14. Bandyopadhyay, S., McGarey, P., et. al, "Conceptual Design of the Lunar Crater Radio Telescope (LCRT) on the Far Side of the Moon," *2021 IEEE Aerospace Conference*, Virtual Conference, March 6-20, 2021.



15. Neal, C. R., Weber, R., Amato, M. J., "The Lunar Geophysical Network (LGN) Decadal Study Final Report," *Presented to the Planetary Decadal Survey Steering Committee and Inner Planets Panel*, August 10, 2020.
16. Colaprete, A., Elphic, R. C., Shirley, M., et. al, "The Volatiles Investigating Polar Exploration Rover (VIPER) Mission," *52<sup>nd</sup> Lunar and Planetary Science Conference*, Virtual Conference, March 15-19, 2021.
17. Gernhardt, M. L., Chappell, S. P., et. al, "NASA's Lunar Terrain Vehicle: Enhancing Crewed and Uncrewed Exploration Via an Unpressurized Mobility Platform," *Lunar Surface Science Workshop (LSSW)*, Virtual Conference, May 28-29, 2020.
18. Bugby, D. C. and Rivera, J. G., "Thermal Technology Advancements for Extended-Duration Lunar Operation," *52<sup>nd</sup> International Conference on Environmental Systems*, ICES-2023-244, July 16-20, 2023.